An Ultra-Low Bending Loss Negative Curvature Hollow Core Fiber With a Polygon Jacketing Layer

Yun-Hao Xu , Dan-Dan Ji , Yuan-Feng Zhu , Yunqi Liu , *Senior Member, IEEE*, Xingfang Luo , Hua Wang , and Xiang-Yu Zuo

Abstract—We design and simulate a new type of hollow-core antiresonant fiber with the polygon jacketing layer. Through numerical calculations, the confinement loss is approximately 0.003 dB/km at 1.45 μm and the bandwidth is $\sim$ 410 nm @ CL $<$ 0.1 dB/km. We found that more nested tubes can be connected to the jacketing layer to avoid the generation of more cladding nodes. The nested tube cladding with the small size of air holes can effectively suppress the coupling between the fiber cladding and core modes even at extreme bending conditions. Ultra-low bending loss is achieved, and the bending loss is lower than $\sim$ 0.05 dB/km @ bend radius $R_b = 3$ cm at 1.50 μm.

Index Terms—Hollow-core fiber, bending losses, surface scattering losses, antiresonant layers.

I. INTRODUCTION

HOLLOW core fibers (HCFs) predominantly confine fiber core modes within the hollow core region, with only a minimal amount of light propagating through the solid fiber materials [1]. Due to the unique structure and guiding mechanism, HCFs break through the inherent limitations of conventional solid fiber. Recently, HCFs have gained extensive utilization in various domains, such as optical communication [2], terahertz wave transmission [3], [4], nonlinear optics [5], [6], high-energy laser transmission [7], and light sensors [8]. This popularity is attributed to their exceptional features, including low latency, low loss, large bandwidth, and high damage threshold [9], [10], [11].

Based on the guidance mechanism, two primary types of HCFs have been documented: hollow-core photonic bandgap fibers (HC-PBGFs) [12] and hollow-core antiresonant fibers (HC-ARFs) [2], [13]. In HC-PBGFs, the photonic bandgaps are achieved through a periodic arrangement of air holes in the fiber cladding [12]. Light at a particular frequency cannot travel through the cladding and becomes trapped in the fiber core. In the case of HC-PBGFs, achieving a low transmission loss is possible, however, the bandwidth is restricted due to the narrow bandgap. Moreover, this type of fiber usually has high group velocity dispersion [14], [15]. HC-ARFs can overcome these problems [16], [17], [18], [19], [20]. The working of HC-ARFs can be described using the antiresonant reflecting optical waveguide (ARROW) model [21], [22], [23]. Optimizing the fiber cladding structures can effectively improve the transmission characteristics of HC-ARF [11]. The large effective refractive index difference between the fiber core and cladding modes ensures the effective transmission of light within these fibers [24], [25], [26], [27]. Currently, researchers are focused on designing and manufacturing negative curvature hollow fibers with low bending loss to mitigate the impact of bending on fiber performance in practical applications.

When an optical fiber is bent, it undergoes resonant coupling between the core fundamental mode and the mode inside one of the cladding capillaries. These resonant couplings can lead to increased bending loss [28]. The bending loss of negative curvature fiber (NCF) can be reduced by changing the sizes of the fiber core and the cladding element as well as by introducing nested cladding elements [29]. Some recent numerical studies have proposed the inclusion of an additional layer of antiresonant tubes into NCFs to create a double-ring geometry [26], [30], [31], [32]. The two-ring split cladding fiber (2SCF) [13] achieves low bending loss by incorporating an inner tube between two outer tubes. By reducing the size of the capillary hole in the second cladding, the interaction between different optical modes during the fiber bending process can be effectively suppressed. Moreover, the coupling between the modes in the fiber core and cladding can be reduced, thereby reducing bending loss. Experiments show that increasing the number of antiresonant layers can reduce the loss [33]. However, introducing additional cladding leads to the emergence of nodes within the cladding, consequently causing increased losses.

The primary objective of this study is to devise a fiber that mitigates the influence of cladding nodes while incorporating an additional layer of the antiresonant tube. We systematically discuss different jacketing layer configurations to identify the influence of different numbers of cladding tubes on the bending

Yun-Hao Xu, Dan-Dan Ji, Yuan-Feng Zhu, Xingfang Luo, and Xiang-Yu Zuo are with the School of Physics and Communication Electronics, Jiangxi Normal University, Nanchang 330022, China, and also with the Key Laboratory of Optoelectronic and Telecommunication of Jiangxi Province, Nanchang 330022, China (e-mail: 202141600172@jxnu.edu.cn; 202141600165@jxnu.edu.cn; yuanfengzhu@jxnu.edu.cn; xfluo@jxnu.edu.cn; 202140100010@jxnu.edu.cn).

Yunqi Liu is with the Key Lab of Specialty Fiber Optics and Optical Access Networks, School of Communication and Information Engineering, Shanghai University, Shanghai 200444, China (e-mail: yqliu@shu.edu.cn).

Hua Wang is with the State Grid Jiangxi Electric Power Corporation, Information and Communication Branch Nanchang, China (e-mail: wanghua@jx.sgcc.com.cn).

Digital Object Identifier 10.1109/JPHOT.2023.3323348
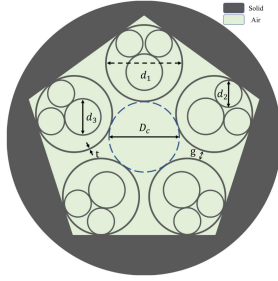
II. DESIGN OF THE FIBER

Fig. 1.   Idealized cross-section of the proposed fiber.

Fig. 2.   (a) False colormaps of confinement loss as a function of d_2/d_1 and d_1/D_c for MN-2SCF with $N = 5$. The other geometrical parameters are set at $D_c = 33$ μm, $t = 0.58$ μm, and $\lambda = 1.40$ μm. (b) Confinement loss as a function of wavelength with respect to d_3.

resistance of fiber. In addition, we investigate the impact of a second inner tube within the nested units on the bending loss. By optimizing the parameters of the cladding structure, ultra-strong bending resistance can be achieved. Our findings indicate that the fiber designed in this manner can markedly decrease bending loss.

II. DESIGN OF THE FIBER

Fig. 1 shows the cross-section of the proposed modified nested 2SCF (MN-2SCF) with a polygonal jacketing layer. Unlike conventional HC-ARFs [31], [32], [33], [34], [35], a tube with a polygonal inner boundary was introduced as the jacketing layer of the fiber. The single-ring HC-ARF with a polygonal jacketing layer has been explored numerically and experimentally [33]. However, to our knowledge, the nested HC-ARF utilizing a polygonal jacketing layer is seldom discussed. Furthermore, compared to the 2SCF, this fiber structure allows for the inclusion of nested anti-resonance layers while introducing as few extra transverse nodes as possible. The additional anti-resonance layer extends the distance from the fiber core to the jacketing layer. It can effectively reduce confinement loss and increase the transmission bandwidth. In the case of the 2SCF, smaller cladding holes can result in reduced bending loss. However, smaller cladding holes also decrease the distance between the fiber core and the sleeve, thereby causing an increase in confinement loss. It is not easy to find a trade-off. While maintaining the larger distance between the fiber core and the jacketing layer, the small size of air holes of the target fiber cladding can effectively prevent the coupling of core mode and cladding mode. Hence, the fiber maintains low bending loss under a small bend radius.

In this work, all fiber structures have a core diameter $D_c = 33$ μm and a glass-web thickness $t = 0.58$ μm. In Fig. 1, the cladding comprises multiple untouched nested tube units surrounding an air core with a diameter of D_c. The number of cladding elements surrounding the core, denoted as N, is constrained to three commonly used cases: N = 4, 5, and 6. Nested tube units are separated by a clearance distance g. Each cladding unit comprises four circular tubes, among which d_1 is the diameter of the outermost tube. Two tubes with a diameter of d_2 are connected to the sheath layer. The tubes with a diameter of d_3 are tangent to two medium tubes with a diameter of d_2, respectively. For the numerical simulations, finite element analysis software (COMSOL) was used, utilizing extremely fine mesh sizes for the
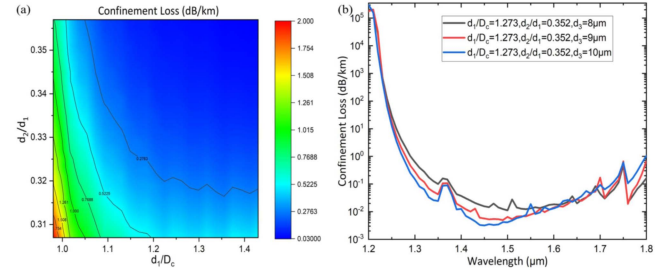
silicon wall and air regions. The calculation region was divided into 400000 segments. All the simulation results were obtained by adding a 6 μm perfect matching layer (PML). Moreover, the maximum mesh size for the finite-element scheme was kept below $\lambda/6$ (where λ is the operating wavelength) for the silica region and $\lambda/4$ for the hollow region as stipulated in this study [18].

In this article, the thickness of the glass-web in all antiresonant units is represented as t, and the refractive index is denoted as n. The resonant wavelength can be determined by (1) given below. The operational wavelength λ is between the high-loss resonant wavelengths.

$$\lambda_{\mathrm{m}} \approx \frac{2t\sqrt{n^2-1}}{m}, m = 1, 2, 3, \ldots \quad (1)$$

The confinement loss (CL) is an essential component of total loss for hollow-core fiber, expressed as follows [23].

$$\alpha_{\mathrm{con}} = \frac{2 \times 10^7}{\ln 10} \frac{2\pi}{\lambda} \mathrm{Im}\left(n_{eff}\right) \quad (dB/m) \quad (2)$$

Surface scattering loss (SSL) is also one of the primary sources of fiber loss. However, for HC-ARF, SSL is usually exceptionally low [18]. Therefore, SSL should only be considered when the CL is very small. The formula of SSL is as follows.

$$\alpha_{\mathrm{sc}}\left[dB/km\right] = \eta F \left(\frac{\lambda\left[\mu m\right]}{\lambda_0}\right)^{-3} \quad (3)$$

where η is a normalization factor, and F is the normalized electric field intensity at the interfaces [18].

III. ANALYSIS OF THE TRANSMISSION CHARACTERISTICS

We first consider the MN-2SCF with five antiresonant tube units. It means $N = 5$, where N is the number of cladding units. Moreover, we assume that the optical fiber parameter $d_2 = d_3$. Fig. 2(a) shows the contour plots of the fundamental mode (FM) CL as a function of normalized tube diameter (d_1/D_c) and normalized nested tube diameter (d_2/d_1). The parameter design area to achieve low loss can be obtained from this figure. It can be seen from the figure that the FM loss remains < 1 dB/km when the $d_1/D_c > 1.08$ and the $d_2/d_1 > 0.315$. Moreover, the CL decreases with the increase of d_2/d_1. With $d_1/D_c = 1.273$ and $d_2/d_1 = 0.352$ set as parameters, Fig. 2(b) shows the CL spectrum with respect to d_3. Optical fiber possesses
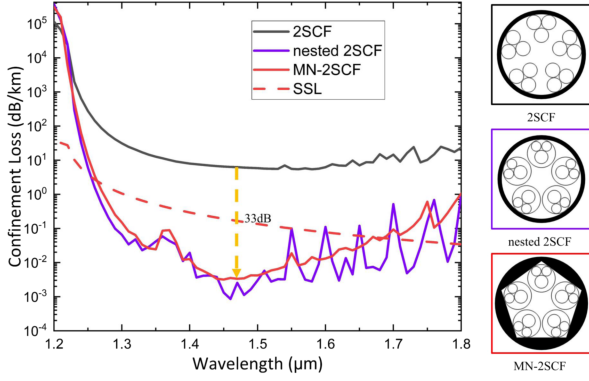
Fig. 3. Confinement losses as a function of wavelength. The solid and dashed lines indicate CLs and SSLs, respectively. The fiber core diameter and glass-web thickness of the three structures are the same, $D_c = 33$ μm and $t = 0.58$ μm, respectively.

the characteristics of a broad bandwidth and low loss. The broadband low-loss characteristics of optical fiber with $d_3 = 10$ μm are superior to those with $d_3 = 8$ μm and 9 μm. The CL of the MN-2SCF with $d_3 = 10$ μm is ~ 0.003 dB/km at the wavelength of 1.45 μm. The respective bandwidth is ~ 410 nm for CL < 0.1 dB/km.

For comparison, we also calculated the loss spectrum of the 2SCF, the nested 2SCF, and the MN-2SCF as shown in Fig. 3. For the 2SCF [13], all tubes are the same size, and the diameter of the dielectric tube to the diameter of the fiber core is 0.621. Parameters of the other two nested structures are $d_1/D_c = 1.273$, $d_2/D_c = 0.448$, and $d_3/D_c = 0.606$. The inclusion of the anti-resonance layer significantly improves the loss performance. However, connecting the circular jacket layer with the nested antiresonant units introduces additional transverse nodes which induce more cladding modes. The couplings between the cladding modes and the core modes result in numerous loss peaks in the spectrum. Instead of a circular jacket layer, using a polygonal jacket layer effectively weakens the adverse impact of cladding nodes. The results show that the CL of the MN-2SCF is 33 dB lower than that of the 2SCF. Additionally, in the wavelength range from 1.27 to 1.67 μm, the CLs are all less than the SSLs.

Group velocity dispersion (GVD) is also an important parameter of optical fibers [3], [20]. The GVD of the MN-2SCF (N = 5) structure is shown in Fig. 4. We can observe that the group velocity dispersion is -28 ps/(nm·km) at a wavelength of 1.3um. Furthermore, there is a minimal change in group velocity dispersion, ranging from -1.94 ps/(nm·km) at 1.4 μm to approximately 1.46 ps/(nm·km) at 1.8 μm.

Next, we extended our investigations to the jacketing layer with different shapes for $N = 4$ and 6. Similar to MN-2SCF with five antiresonant tube units, we initially assumed that the optical fiber parameter $d_2 = d_3$. Fig. 5(a) and (b) show contour plots of the fundamental mode CL as a function of d_1/D_c and d_2/d_1. Optical fiber with $N = 4$ or 6 also has low loss characteristics. The fundamental mode CLs are 0.0135 dB/km and 0.192 dB/km for the fiber with $N = 4$ ($d_1/D_c = 2.12$, $d_2/d_1 = 0.4$) and $N = 6$ ($d_1/D_c = 0.96$, $d_2/d_1 = 0.318$), respectively. The smaller the value of N, the greater the design parameter space available to achieve low
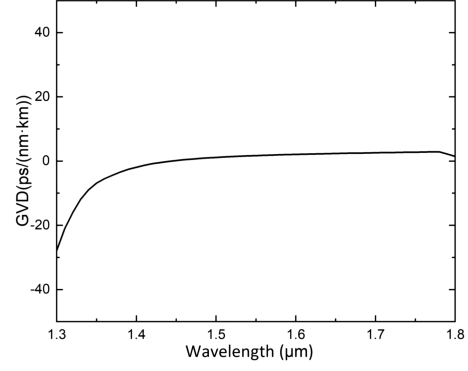

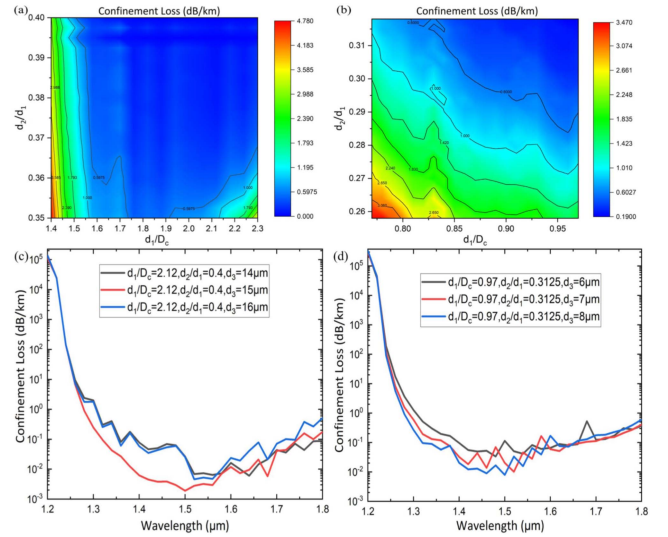Fig. 4. Group velocity dispersion as a function of wavelength for MN-2SCF (N = 5).

Fig. 5. (a) and (b) false colormaps of confinement loss as a function of d_2/d_1 and d_1/D_c for MN-2SCF with $N = 4$ and $N = 6$. The other geometrical parameters are set at $D_c = 33$ μm, $t = 0.58$ μm, and $\lambda = 1.40$ μm. (c) Confinement loss as a function of wavelength for MN-2SCF ($N = 4$) with $d_1/D_c = 2.12$ and $d_2/d_1 = 0.4$. (d) Confinement loss in the fundamental mode as a function of wavelength for MN-2SCF ($N = 6$) with $d_1/D_c = 0.97$ and $d_2/d_1 = 0.3125$.

loss. Fig. 5(c) and (d) show the CL spectrum with different values of d_3. The fiber with different shape jacketing layers also shows wide bandwidth and low loss characteristics. In addition, we can further reduce the loss and increase the bandwidth by optimizing the value of d_3. Fibers featuring square and pentagonal jacketing layer structures show lower loss values than structures with hexagonal jacketing layers. This phenomenon can be attributed to the fact that a smaller value of N allows for a larger selection of normalized parameter d_1/D_c to construct the optical fiber. Consequently, there is a greater distance between the fiber core and the jacketing layer, resulting in lower fundamental mode CL for the fiber. Moreover, loss oscillations induced by the couplings between the cladding and the core modes are significantly attenuated throughout the transmission band [19]. The CL of the MN-2SCF (N = 4) with $d_1/D_c = 2.12$, $d_2/d_1 = 0.4$ and $d_3 = 15$ μm is ~ 0.0018 dB/km at the wavelength of 1.50 μm. Furthermore, the bandwidth is ~ 420 nm for CL < 0.1 dB/km.
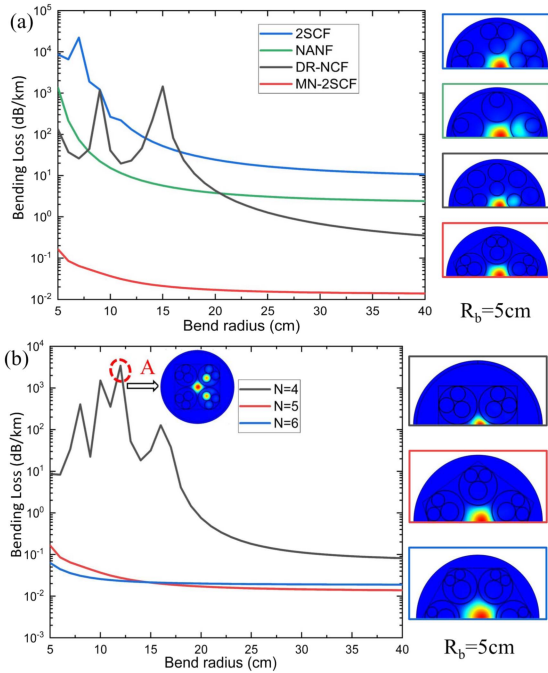
Fig. 6. (a) Relationship between bending loss and bending radius of different structures. Any other structural parameters are optimized as identified in their respective reports. (b) The relationship between bending loss and bending radius of clamp tubes with different shapes. On the right is the corresponding field distribution for $R_b = 5$ cm with the following set of parameters. $N = 4$, $d_1/D_c = 2.12$ and $d_2/d_1 = 0.4$, $d_3 = 15\mu$m. $N = 5$, $d_1/D_c = 1.273$ and $d_2/d_1 = 0.352$, $d_3 = 10\mu$m. $N = 6$, $d_1/D_c = 0.97$ and $d_2/d_1 = 0.3125$, $d_3 = 8\mu$m.

IV. BENDING CHARACTERISTICS ANALYSIS

Since optical fibers must be installed in different environments, their resilience to external disturbances is worth investigating. Here, we investigate the bending loss characteristic of MN-2SCF. The bending of the fiber can be simulated by a straight fiber with a modified refractive index profile [18]. A useful quantity n_{eq} is the equivalent refractive index defined as follows. $n_{eq} = n(x, y)[1+(xcos\theta+ysin\theta)/R_b]$. $n(x, y)$ is the refractive index distribution of the straight fiber. R_b is the radius of curvature, and θ is the angle between the bending direction of the fiber and the x-axis.

Assume that $\theta = 0°$ along the x-axis represents the bending direction. The functional relationships between the bending loss and bending radius of nested antiresonant nodeless HC fiber (NANF), 2SCF, double ring negative curvature fiber (DR-NCF) [26] and MN-2SCF at the wavelength of 1.4 μm are shown in Fig. 6(a). As observed, the bending loss gradually increases as the bending radius decreases. Due to the coupling effects between core and cladding modes [28], bending loss peaks of 2SCF and DR-NCF can be seen in Fig. 6(a). However, for MN-2SCF, this coupling effect does not manifest. When the bending radius is 5 cm, MN-2SCF ($N = 5$) shows good bending performance. The bending loss of MN-2SCF ($N = 5$) is about 4–5 orders lower than those of NANF and 2SCF and about 2–3 orders lower than that of DR-NCF. Analogously, we turn our attention to fiber structures with different shapes of jacketing layer, where the values of D_c and t are consistent. Fig. 6(b)
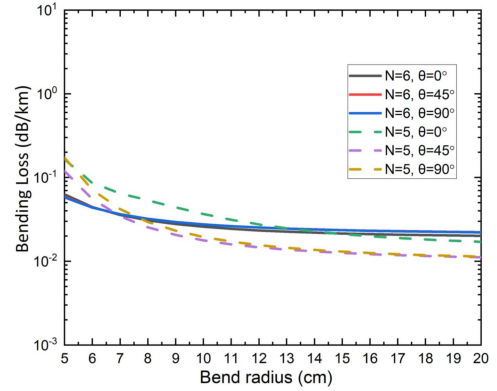

Fig. 7. Bending losses of MN-2SCF ($N = 5$ and $N = 6$) in different bending directions. The structure parameters are consistent with those in Fig. 5.

shows that the proposed fibers with pentagonal and hexagonal structures show favorable bending loss performance at small bending radii. Specifically, for hexagonal structures, at a bending radius of 5 cm, the bending loss of the fiber is merely 0.06 dB/km. In addition, under compact bending, the bending loss of optical fiber with a square structure is notably higher than the other two types. It is attributed to the substantial gap between the capillaries along the x-axis and the mode coupling induced by the bend, as indicated by point A in the figure. The insets in Fig. 6(b) show the electric field distribution of the fundamental mode at $R_b = 5$ cm. Due to the large bending loss of square structure optical fiber, we will discuss the bending loss characteristics of the pentagonal and hexagonal structures optical fibers in the following discussion.

Next, we discuss the bending losses of MN-2SCF ($N = 6$ and $N = 5$) in different bending directions, as shown in Fig. 7. It can be seen that when $N = 6$, there is no significant difference in bending losses in different bending directions. For $N = 5$, $\theta = 0°$, $\theta = 45°$, and $\theta = 90°$ corresponding bending losses are 0.165 dB/km, 0.119 dB/km, and 0.171 dB/km at $R_b = 5$cm. The bending losses at $\theta = 45°$ and $\theta = 90°$ are less than those with $\theta = 0°$ when the bending radius is greater than 5.5cm. Overall, the bending losses caused by bending in different directions are not significantly different. Therefore, in the following analysis, the bending direction is set to be the x direction.

Fig. 8 illustrates the bending-induced losses versus wavelength for $R_b = 3$, 5, and 7 cm. As shown in Fig. 8, the bending loss decreases as the bending radius increases, as expected. At $R_b = 3$ cm, bending induces resonant coupling between the FM and the cladding mode at the wavelength of 1.4 μm for the pentagon jacketing layer structure, resulting in light leakage from the core. A fiber with a hexagonal structure demonstrates superior anti-bending performance compared to one with a pentagon structure at $R_b = 3$ cm. The bending loss of the hexagonal jacketing layer structure can be kept below 1 dB/km, covering the wavelength from 1.4 μm to 1.55 μm. When $R_b = 7$ cm, the bending loss of the pentagon structure fiber reaches 0.013 dB/km at the wavelength of 1.5 μm. Moreover, the bandwidth is $\sim$ 310 nm for BL < 0.1 dB/km, showing excellent anti-bending performance.
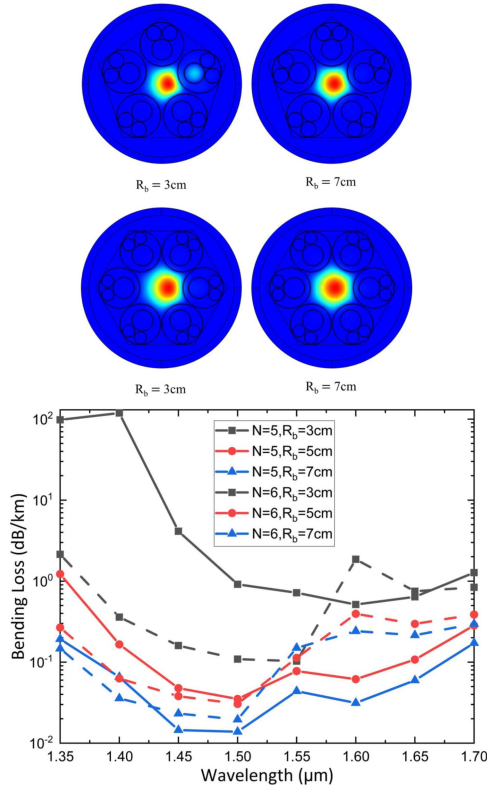
Fig. 8. Bending loss performance of pentagonal and hexagonal structure fibers under different bending radii. The structure parameters are consistent with those in Fig. 6. The corresponding FM field profiles are given in the upper inset.

Fig. 9. False colormaps of bending loss against d_3/D_c and R_b for $N = 5$(a) and $N = 6$(b), respectively. The insets in (a) and (b) show the electric power profiles of the FM for different d_3/D_c values.

Fig. 10. Bending loss performance of the hexagonal structure fiber under different bending radii R_b with $d_1/D_c = 0.97$, $d_2/d_1 = 0.3125$, and $d_3 = 7.6$ μm. The solid and dashed lines indicate BLs and surface scattering losses (SSLs).

Next, we discuss the effect of the parameter d_3/D_c on the bending loss. Fig. 9(a) and (b) are the false color maps of the bending loss for MN-2SCF with R_b in the horizontal axis and d_3/D_c in the vertical axis for $N = 5$ and 6, respectively. When the R_b and d_3/D_c values are both small, the optical fibers for $N = 5$ and 6 have a loss peak caused by resonance coupling between modes in the fiber core and the cladding, respectively. The cladding mode is located at the air hole between diameter d_3 and diameter d_1 tubes. It is discerned in the inset labeled III in Fig. 9(a) and (b). For $N = 5$, with the increase of d_3/D_c, there are two high-loss regions labeled I and II related to the bending-induced resonant coupling between the FM and the cladding mode in the tube with diameter d_3. The electric field profiles of the hybrid mode are shown in the insets labeled I and II in Fig. 9(a). The most apparent characteristic is that the resonant couplings between the FM and cladding modes occur only at conditions of relatively small R_b, especially for $N = 6$. It is because all individual air holes within the cladding elements are reduced in size due to the presence of multiple nested tubes, causing the effective indices of the modes in cladding holes to be significantly lower than that of the FM in the fiber core. Hence, it is difficult to satisfy the resonance coupling condition even under tight bending distortion, making it more resistant to bending. The fiber has a broad range of low bending loss for BL < 0.1 dB/km and exhibits better bending loss characteristics when $d_3/D_c = 0.47$. The bending-induced loss of 0.1 dB/km can be achieved for R_b as low as 4.3 cm.
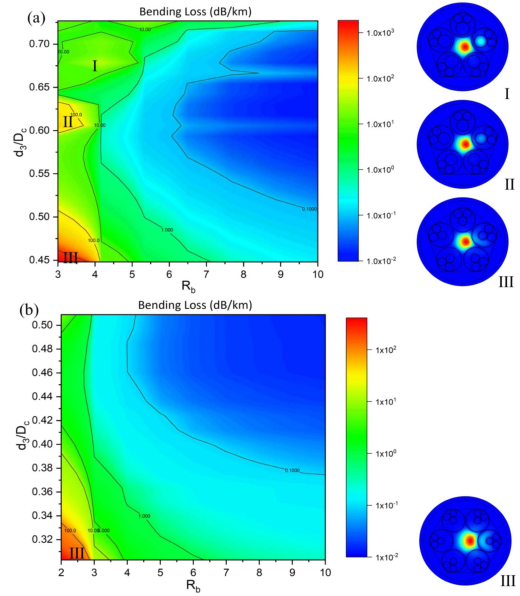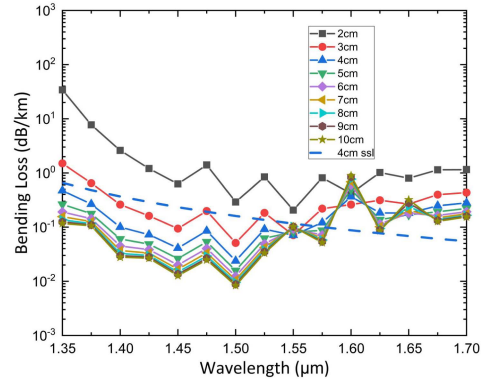
By modifying the cladding structure parameters, various bending radii are considered to investigate the variations in bending loss characteristics with wavelength (Fig. 10). It is noticed from Fig. 10 that even if the bending radius is minimal, the optical energy can be well-confined to the core. When R_b = 3 cm, the bending loss of MN-2SCF ($N = 6$) at 1.50 μm is 0.05 dB/km, and the total loss (total loss is the sum of SSLs and BLs) of the fiber is 0.688 dB/km. It can also be seen that when the bending radius becomes larger than 4 cm, the bending loss is less than 1 dB/km for the wavelength from 1.35 μm to 1.56 μm. On the other hand, the SSL of the optical fiber with a bending radius of 4 cm is also calculated. It can be seen from the figure that the bending loss of MN-2SCF is lower than that of SSL for the wavelength from 1.35 μm to 1.56 μm. As shown in Fig. 10, the fiber can maintain a low bending loss within a broad bandwidth even under extreme bending conditions.

TABLE I
PARAMETERS IN NEGATIVE CURVATURE FIBERS

| Ref. (Year)	Confinement Loss	Transmission Window	Bending Loss
[2] (2018)	2 dB/km at 1.512μm	16 dB/km for 335 nm	<1 dB/km for R_b = 10 cm
[23] (2019)	1.3 dB/km at 1.45 μm	2 dB/km for 90 nm	<0.1 dB/km
[3] (2021)	0.0037 dB/km at 1.06 μm	< 0.1 dB/km over 160 nm	~ 0.44 dB/km for R_b = 5 cm
[31] (2022)	0.008 dB/km at 1.06 μm	< 1 dB/km over 200 nm	~ 2 dB/km for R_b > 40 cm
[32] (2023)	0.0066 dB/km at 1.52 μm	< 0.1 dB/km for 630 nm	~ 0.08 dB/km for R_b = 15 cm
This Work	0.003 dB/km at 1.45 μm	<0.1 dB/km for 420 nm	~ 0.05 dB/km for R_b = 3 cm
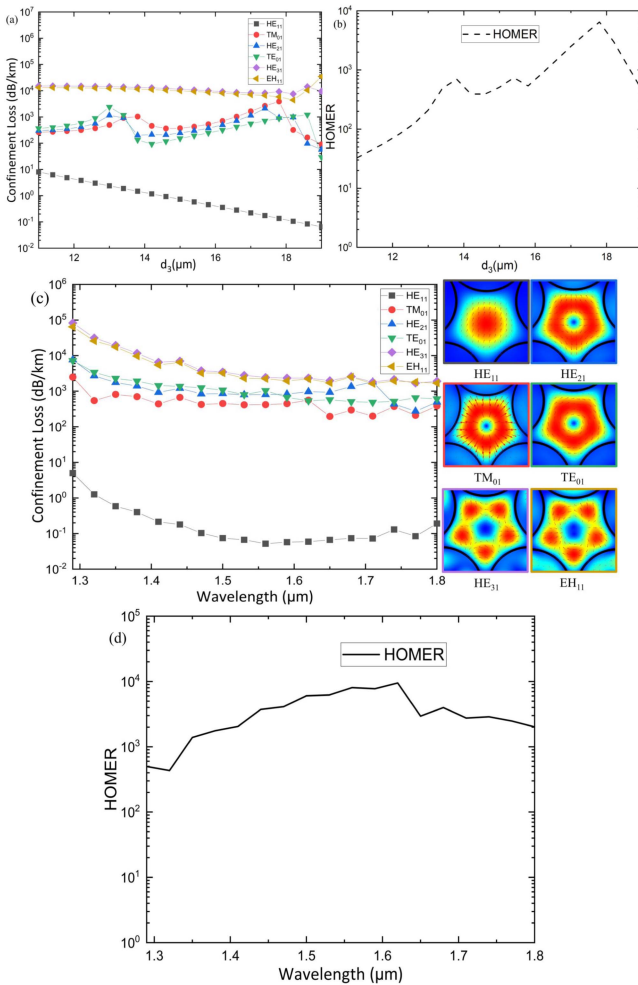
Fig. 11. (a) CL and (b) HOMER at different d_3. (c) CL at different wavelengths with $d_3 = 17\mu$m. On the right are the mode fields for each core mode. (d) HOMER at different wavelengths with $d_3 = 17\mu$m.

Theoretical performance comparisons between the fiber investigated in this study and several reported fibers are presented in Table I, covering a comparison of confinement loss and bending loss. It can be found that the fiber proposed in this work also has a larger low-loss transmission bandwidth due to the multiple antiresonant layers and few nodes in the cladding. It should be emphasized that the fiber exhibits excellent quality in terms of low bending loss. Compared with other fiber structures, the bending losses are improved to a substantial extent at small bending radii.

V. SINGLE-MODE PERFORMANCE

We analyze the single-mode performance of the proposed MN-2SCF ($N = 5$) in this section. High order mode extinction ratio (HOMER) can be used to evaluate the single mode performance of MN-2SCF. It is defined as the ratio between the high order mode (HOM) with the lowest loss and the loss of FM [18]. We discuss the characteristics of the HE_{11}, TE_{01}, HE_{21}, TM_{01}, EH_{11}, and HE_{31} modes [26]. The optical fiber structure parameters were set as follows: $D_c = 33$ μm, $d_1 = 44.8$ μm, $d_2 = 12$ μm, and $\lambda = 1.4$ μm. Fig. 11(a) shows the relationship between CLs for fiber core modes and d_3. By appropriately changing the structural parameter d_3, strong coupling can occur between the cladding modes and HOMs, resulting in a larger HOMER value. When d_3 increases from 12.5μm to 18μm in Fig. 11(b), HOMER is all greater than 100. Fig. 11(c) shows the relationship between the CLs of fiber modes and wavelength, with $d_3 = 17\mu$m. In the broad bandwidth, the CLs of all HOMs are all much higher than those of the FM. The HOMER is calculated using the CLs of TM_{01}, which are the lowest loss of HOMs as shown in Fig. 11(c). The highest HOMER of about 9500 is found around 1.62 μm, and the value remains greater than 1000 over the range from 1.35μm–1.8μm as seen in Fig. 11(d).

VI. CONCLUSION

In summary, a new HC-ARF with a polygonal jacketing layer was proposed. In this optical fiber structure, multiple dielectric tubes in the antiresonant unit were directly connected to the outer polygon jacketing layer, effectively avoiding the increase of cladding nodes while increasing the antiresonant layers. We studied the impact of various jacketing layer shapes on bending loss, observing that the pentagonal and hexagonal jacketing layers exhibit outstanding bending loss performances. The bending loss of the hexagonal structure was 0.05 dB/km at a bending radius of 3 cm.

REFERENCES

[1] R. F. Cregan et al., "Single mode photonic band gap guidance of light in air," *Science*, vol. 285, no. 5433, pp. 1537–1539, Sep. 1999.

[2] S. F. Gao et al., "Hollow-core conjoined-tube negative-curvature fibre with ultralow loss," *Nature Commun.*, vol. 9, Jul. 2018, Art. no. 2828.

[3] H. Pakarzadeh, S. M. Rezaei, and L. Namroodi, "Hollow-core photonic crystal fibers for efficient terahertz transmission," *Opt. Commun.*, vol. 433, pp. 81–88, Feb. 2019.

[4] V. Sharif and H. Pakarzadeh, "Terahertz hollow-core optical fibers for efficient transmission of orbital angular momentum modes," *J. Lightw. Technol.*, vol. 39, no. 13, pp. 4462–4468, Jul. 2021.

[5] M. Azhar, G. K. L. Wong, W. Chang, N. Y. Joly, and P. S. J. Russell, "Raman-free nonlinear optical effects in high pressure gas-filled hollow core PCF," *Opt. Exp.*, vol. 21, no. 4, pp. 4405–4410, Feb. 2013.

[6] W. H. Renninger, R. O. Behunin, and P. T. Rakich, "Guided-wave Brillouin scattering in air," *Optica*, vol. 3, no. 12, pp. 1316–1319, Dec. 2016.

[7] G. Humbert et al., "Hollow core photonic crystal fibers for beam delivery," *Opt. Exp.*, vol. 12, no. 8, pp. 1477–1484, Apr. 2004.

[8] F. Benabid, P. J. Roberts, F. Couny, and P. S. Light, "Light and gas confinement in hollow-core photonic crystal fibre based photonic microcells," *J. Eur. Opt. Soc.*, vol. 4, no. 4, Jan. 2009, Art. no. 09004.

[9] P. S. J. Russell, P. Hölzer, W. Chang, A. Abdolvand, and J. C. Travers, "Hollow-core photonic crystal fibres for gas-based nonlinear optics," *Nature Photon.*, vol. 8, no. 4, pp. 278–286, Apr. 2014.

[10] X. Liu et al., "Characterization of a liquid-filled nodeless anti-resonant fiber for biochemical sensing," *Opt. Lett.*, vol. 42, no. 4, pp. 863–866, Feb. 2017.

[11] C. Wei, R. Joseph Weiblen, C. R. Menyuk, and J. Hu, "Negative curvature fibers," *Adv. Opt. Photon.*, vol. 9, no. 3, pp. 504–561, Sep. 2017.

[12] J. C. Knight, J. Broeng, T. A. Birks, and P. S. J. Russell, "Photonic band gap guidance in optical fibers," *Science*, vol. 282, no. 5393, pp. 1476–1478, Nov. 1998.

[13] X. Huang, W. Qi, D. Ho, K. T. Yong, F. Luan, and S. Yoo, "Hollow core anti-resonant fiber with split cladding," *Opt. Exp.*, vol. 24, no. 7, pp. 7670–7678, Apr. 2016.

[14] X. Zhang, S. Gao, Y. Wang, W. Ding, X. Wang, and P. Wang, "7-cell hollow-core photonic bandgap fiber with broad spectral bandwidth and low loss," *Opt. Exp.*, vol. 27, no. 8, pp. 11608–11616, Apr. 2019.

[15] P. Roberts et al., "Ultimate low loss of hollow-core photonic crystal fibres," *Opt. Exp.*, vol. 13, no. 1, pp. 236–244, Jan. 2005.

[16] W. Belardi and J. C. Knight, "Hollow antiresonant fibers with reduced attenuation," *Opt. Lett.*, vol. 39, no. 7, pp. 1853–1856, Apr. 2014.

[17] W. Belardi and J. C. Knight, "Hollow antiresonant fibers with low bending loss," *Opt. Exp.*, vol. 22, no. 8, pp. 10091–10096, Apr. 2014.

[18] F. Poletti, "Nested antiresonant nodeless hollow core fiber," *Opt. Exp.*, vol. 22, no. 20, pp. 23807–23828, Oct. 2014.

[19] M. S. Habib, O. Bang, and M. Bache, "Low-loss hollow-core silica fibers with adjacent nested anti-resonant tubes," *Opt. Exp.*, vol. 23, no. 13, pp. 17394–17406, Jun. 2015.

[20] W. Belardi, "Design and properties of hollow antiresonant fibers for the visible and near infrared spectral range," *J. Lightw. Technol.*, vol. 33, no. 21, pp. 4497–4503, Nov. 2015.

[21] N. M. Litchinitser et al., "Resonances in microstructured optical waveguides," *Opt. Exp.*, vol. 11, no. 10, pp. 1243–1251, May 2003.

[22] M. A. Duguay, Y. Kokubun, T. L. Koch, and L. Pfeiffer, "Antiresonant reflecting optical waveguides in SiO_2-Simultilayer structures," *Appl. Phys. Lett*, vol. 49, no. 1, pp. 13–15, Jul. 1986.

[23] T. P. White et al., "Multipole method for microstructured optical fibers, I. Formulation," *J. Opt. Soc. Amer. B*, vol. 19, no. 10, pp. 2322–2330, Oct. 2002.

[24] L. Vincent and V. Setti, "Waveguiding mechanism in tube lattice fibers," *Opt. Exp.*, vol. 18, no. 22, pp. 23133–23146, Oct. 2010.

[25] Y. Y. Wang, N. V. Sheeler, F. Couny, P. J. Roberts, and F. Benabid, "Low loss broadband transmission in hypocycloid-core Kagome hollow-core photonic crystal fiber," *Opt. Lett.*, vol. 36, no. 5, pp. 669–671, Mar. 2011.

[26] Y. X. Wang, M. I. Hasan, M. R. A. Hassan, and W. Chang, "Effect of the second ring of antiresonant tubes in negative curvature fibers," *Opt. Exp.*, vol. 28, no. 2, pp. 1168–1176, Jan. 2020.

[27] T. D. Bradley et al., "Record low-loss 1.3 dB/km data transmitting antiresonant hollow core fibre," in *Proc. Eur. Conf. Opt. Commun.*, 2018, pp. 1–3.

[28] M. H. Frosz, P. Roth, M. C. Günendi, and P. S. J. Russell, "Analytical formulation for the bend loss in single-ring hollow-core photonic crystal fbers," *Photon. Res.*, vol. 5, no. 2, pp. 88–91, Apr. 2017.

[29] Y. Wang and W. Chang, "Understanding bending-induced loss and bending-enhanced higher-order mode suppression in negative curvature fibers," *Opt. Exp.*, vol. 29, no. 15, pp. 23622–23626, Jul. 2021.

[30] X. Huang, S. Y. oo, and K. T. Yong, "Function of second cladding layer in hollow-core tube lattice fibers," *Sci. Rep.*, vol. 7, no. 7, May 2017, Art. no. 1618.

[31] S. Yan, S. Lou, W. Zhang, and Z. Lian, "Single-polarization single-mode double-ring hollow-core anti-resonant fiber," *Opt. Exp.*, vol. 26, no. 24, pp. 31160–31171, Nov. 2018.

[32] X. Chen et al., "Double negative curvature anti-resonance hollow core fiber," *Opt. Exp.*, vol. 27, no. 14, pp. 19548–19554, Jul. 2019.

[33] M. Alharbi et al., "Hypocycloid-shaped hollow-core photonic crystal fiber Part II: Cladding effect on confinement and bend loss," *Opt. Exp.*, vol. 21, no. 23, pp. 28609–28616, Nov. 2013.

[34] B. Yang et al., "Low loss hollow-core connecting-circle negative-curvature fibres," *IEEE Photon. J.*, vol. 13, no. 1, Feb. 2021, Art. no. 7200710.

[35] Y. Zhou et al., "A negative-curvature hollow-core fiber structure with double trigonal-symmetrical anti-resonant elements," *IEEE Photon. J.*, vol. 14, no. 1, Feb. 2022, Art. no. 7910306.

[36] Y.-F. Zhu, X.-Y. Zuo, P. Yan, D.-D. Ji, Y.-H. Xu, and X. Luo, "Low-loss nodeless conjoined-tube anti-resonant hollow-core fiber," *J. Lightw. Technol.*, vol. 41, no. 14, pp. 4831–4839, Jul. 2023.